

# Nuclear burning and mixing in the first stars: entrainment at a convective boundary using the PPB advection scheme

Paul Woodward\*, Falk Herwig<sup>†,\*\*</sup>, David Porter\*, Tyler Fuchs\*, Anthony Nowatzki\* and Marco Pignatari<sup>†</sup>

\*Laboratory for Computational Science & Engineering, University of Minnesota, USA

<sup>†</sup>Astrophysics Group, School of Physical and Geographical Sciences, Keele University, UK

\*\*T-Division, Los Alamos National Laboratory, Los Alamos, NM, USA (Affiliate)

**Abstract.** The evolution of the first generations of stars at zero or extremely low metallicity, and especially some crucial properties like the primary  $^{14}\text{N}$  production, is characterized by convective-reactive mixing events that are mostly absent from similar evolution phases at solar-like metallicity. These episodes occur when unprocessed H-rich material is mixed across a convective boundary into  $^{12}\text{C}$  rich He-burning material, as for example in He-shell flashes of extremely-low metallicity AGB stars. In this paper we describe the astrophysical context of such convective-reactive events, including the difficulty of current one-dimensional stellar evolution models to correctly simulate these evolutionary phases. We then describe the requirements and current state of modeling convective-reactive processes in the first stars environment. We demonstrate some of the new concepts that we are applying to this problem, i.e. the highly accurate PPB advection scheme in the framework of PPM hydrodynamic simulations of mixing across a very stiff convective boundary. We show initial results of such simulations that address the first non-reactive step of this problem, which is the entrainment of H at the top boundary of the He-shell flash convection zone.

**Keywords:** first stars: nucleosynthesis, mixing, hydrodynamics

**PACS:** 95.30.Lz, 95.30.Tg, 95.75.Pq, 97.10.Cv, 97.20.Li, 97.20.Wt

## INTRODUCTION

The formation and evolution of the first generations of stars traces the formation and evolution of the first structure on cosmological scales (e.g. O’Shea, this volume), and starts the continuing process of chemical evolution in galaxies. The nuclear production in these stars provides an important tracer of events that took place in the early Universe [e.g. 1]. An increasing number of very metal-poor stars ( $[\text{Fe}/\text{H}] < -2$ ) are now discovered in large spectroscopic surveys [2] reaching down to metallicities below  $[\text{Fe}/\text{H}] = -5$  [3]. These low-mass stars preserve the signature of the nuclear processes in the first generations of stars, of both low mass as well as from massive stars. Some important findings from the observational study of stars that carry the signature of the first generations of stars include the following.

The fraction of C-enhanced stars ( $[\text{C}/\text{Fe}] > 1$ ) is between about 10% [4] and 20% [5] for stars with  $[\text{Fe}/\text{H}] < -2$ , and increases with decreasing metallicity. Below  $[\text{Fe}/\text{H}] < -3$  there are now about 300 C-rich stars, below  $[\text{Fe}/\text{H}] < -3.5$  40% are C-rich. 80% of these CEMP stars are enhanced with s-process elements [6, 7]. Many of these CEMP-s stars show evidence for binarity and Lucatello et al. [8] find that present data is statistically consistent with all CEMP-s stars being in binaries. The abundance signature of this large group of CEMP-s stars has been interpreted as being the result of mass trans-

fer from an Asymptotic Giant Branch (AGB) star, that is now a white dwarf. An additional important finding is that CEMP-s stars have C to N ratios that are slightly lower than predicted by non hot-bottom burning, low-mass, third dredge-up AGB stars ( $0 \leq [\text{C}/\text{N}] \leq 1.5$ ), but about 2 orders of magnitude larger than any hot-bottom burning AGB models [9].

As far as heavy elements are concerned one of the most remarkable findings is the discovery of the solar-scaled, apparently universal r-process element distribution for the heavy neutron capture elements,  $56 \leq Z < 83$  [10]. However, for lower elemental mass down to Sr the observed element abundance distribution in several extremely metal poor stars can not be only accounted for by the standard solar-scaled r-process. Since at very low metallicity the average contribution from the weak and main s process is negligible, an extra contribution from a primary s process called light element primary process (LEPP) has been proposed [11]. Recently, Montes et al. [12] showed that the LEPP signature at very low metallicity could be reproduced by a process with neutron densities of less than  $10^{13}\text{cm}^{-3}$ , which are intermediate between the typical s- (much lower) and r-process (much higher). Concerning the light elements, the observations of extremely metal poor stars of any variety point at a primary production of  $^{14}\text{N}$  that is currently not yet well understood [e.g. 13].

These observational findings of the first generations

of stars, that have been discussed at length at this First Stars III conference, have one thing in common. They are sensitively related to the physics of mixing, and in some cases the hydrodynamic interaction of mixing and nuclear burning. The present 1-D spherically symmetric stellar evolution models of these low-metallicity stars do not account properly for this physics. While this is true also for solar-like metallicity, the uncertainties are amplified by the flash-like burning of H mixed into  $^{12}\text{C}$ -rich He-burning layers. As we will describe below these convective-reactive events are peculiar to extremely low-metallicity stellar conditions. Uncertainty in mixing is not limited to convection-induced mixing of course. Rotation must play an important role. The uncertainty of present rotating stellar models is evident from their inability to properly meet constraints from pulsars [14, 15] in the case of massive stars models, or the inhibiting effect of rotation in simulations of the s process in low-mass stars [16]. However, some areas related to the comparatively fast and dynamic evolution of convective and convective-reactive events in the stellar interior are open to detailed hydrodynamic simulations. In the following sections we will discuss the discussed observational properties of the extremely metal poor stars in the framework of one-dimensional stellar evolution simulations with the goal to identify the most promising, high-gain situations in first stars that can be investigated by hydrodynamical simulations now. We will discuss the one-dimensional spherically symmetric assumption in the convective-reactive cases. We will then present some new simulations of one of these important convective boundaries, showcasing the PPB advection scheme at work inside the most recent version of the LCSE PPM stellar hydrodynamics code. Finally we report high-resolution simulations of the top convective boundary of He-shell flash convection. Mixing at this boundary determines the properties if the H-ingestion flash in EMP AGB stars.

## STELLAR EVOLUTION AT ZERO OR EXTREMELY LOW METALLICITY

### Hot-bottom burning and hot dredge-up

In the Introduction we have summarized the observational properties of the CEMP-s stars. Low-mass AGB stars below  $2M_{\odot}$  are indeed expected to produce C- and s-rich abundance signatures even at extremely low metallicity [e.g. 17]. But slightly more massive primaries would have experienced the third dredge-up *and* hot-bottom burning with a characteristically low C/N ratio in the ejecta. According to Campbell’s grid calculation [18, 19] at an iron content of  $[\text{Fe}/\text{H}] \leq -3$  all models

with  $M \geq 2M_{\odot}$  show at the surface the CNO equilibrium value  $[\text{C}/\text{N}] \sim -2$  because of hot-bottom burning. From this it follows that if CEMP stars result from AGB binary mass transfer we should expect also a certain number of N-enhanced metal poor (NEMP) stars. Johnson et al. [9] have searched for these NEMP stars, looking especially into possible selection effects and observable biases. They did not find a single NEMP star in their targeted investigation. Uncertainties in the treatment of mixing in one-dimensional models rather exacerbate the problem as they include possibilities to produce N even more efficiently at lower metallicity.

At face value standard stellar evolution predicts that the nucleosynthetic source of the abundance signature in CEMP-s stars (or any CEMP star thought to be polluted by a former AGB companion with  $[\text{C}/\text{N}] > 0.0$ ) can only come from stars with initial masses less than  $2M_{\odot}$ . The exact value of this limiting mass including the metallicity dependence still needs to be determined. It depends on the physics of mixing in at least two ways. One is through the mixing length parameter used in the convective envelope. Most standard stellar evolution calculations use the solar scaled mixing length parameter also during the AGB phase. In their text book Cox and Giuli [20, Ch. 14.3] recommend a mixing length parameter of 1.5 for a solar-type convection zone, and about 2.1 for a red-giant type convection zone. A larger mixing-length parameter for AGB stars is also resulting from full hydrodynamic simulations by Porter and Woodward [21,  $\alpha_{\text{MLT}} = 2.7$ ] as well as the majority of semi-empirical, observations based determinations [22,  $\alpha_{\text{MLT}} = 2.2 \dots 2.6$ ]<sup>1</sup>. A larger mixing-length parameter leads to more vigorous envelope burning, and further decreases the limiting initial mass of envelope burning. An update of the work by Porter and Woodward [21] for the low masses and metallicities relevant here, and the application of these results to one-dimensional stellar evolution calculations would greatly enhance the accuracy of the determination of the limiting mass for hot-bottom burning in EMP AGB stars.

The other mixing process that affects N production in low-mass AGB stars is any mixing at or across the bottom boundary of the convective envelope. The slightly reduced observational  $[\text{C}/\text{N}]$  ratios compared to low-mass predictions may hint at some mixing processes below the convective envelope. Clearly, the whole radiative  $^{13}\text{C}$ -pocket based s-process concept [23] is built on mixing of H across the convective boundary into the  $^{12}\text{C}$ -rich core. Whatever the physical cause is of these convection-induced extra-mixing processes, it may easily enhance the hot-bottom burning efficiency. This ques-

<sup>1</sup> In both cases mixing-length parameters were determined in the MLT version of Cox and Giuli [20].

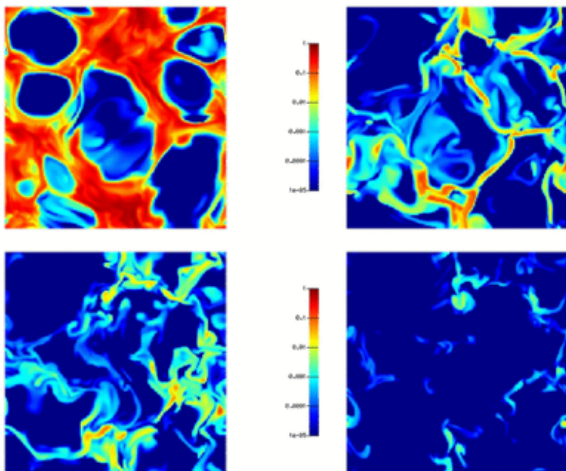


**FIGURE 1.** A snapshot of the abundance of H-rich material (red, originally only in the radiative layer) in a HIF toy simulation. The panels show horizontal planes (from left to right and top to bottom: just above the top convective boundary, and at three successively deeper location inside the convectively unstable layer) from an underresolved ( $150^2 \times 100$ ) three-dimensional RAGE simulation of He-shell flash convection. The setup and stratification is similar to Herwig et al. [26], with a much enhanced energy driving for the convection. Convective boundaries are not resolved, nevertheless the simulation demonstrates one of the reasons why convective-reactive events need to be investigated in the multi-dimensional hydrodynamic rather than one-dimensional, spherically symmetric framework, as discussed in the text.

tion can be investigated with some numerical experiments similar to the one we present in the next section.

Modeling the production of C, N and s-process element production in EMP AGB stars poses more challenges related to the mixing during the third dredge-up. As we just mentioned, this mixing plays an essential role in the formation of the  $^{13}\text{C}$  pocket. What are the properties of this mixing in EMP AGB stars? Recent studies [24, 25] have shown that even small amounts of mixing at the bottom boundary of the convective envelope in intermediate mass stars ( $4$  and  $5 M_{\odot}$ ) can lead to possibly violent, even eroding or excavating, flame-like burning.

Fig. 4 in Goriely and Siess [27] demonstrates how the temperature at the base of the convective envelope increases with mass and decreasing metallicity, exceeding at  $[\text{Fe}/\text{H}] = -2.3$   $6 \cdot 10^7$  K for  $4 M_{\odot}$  and  $8 \cdot 10^7$  K for  $5 M_{\odot}$ . In that work it is described how the amount of mixing across the convective boundary that is associated with the formation of a  $^{13}\text{C}$  pocket for the s process at solar metallicity does not lead to a formation of s-process elements at extremely low metallicity, due to instantaneous burning of protons in the *hot* third dredge-up of a  $3 M_{\odot}$ ,  $Z=0.0001$  case. Herwig [25, Fig. 7]

shows how this hot dredge-up can feed back into the stellar structure and explain how this mixing, depending on its efficiency leads to very deep, eroding dredge-up. Mixing at this boundary with only a quarter of the efficiency that is deduced from s-process observations for low-mass, solar metallicity stars [28] would within 2000 yr completely eject the entire envelope through a high-luminosity ( $\log L/L_{\odot} \sim 5$ ) driven superwind with mass loss rates of a few  $10^{-3} M_{\odot}/\text{yr}$ . The luminosity during the hot dredge-up and the consequences for the structural evolution and s process depend sensitively on the mixing efficiency at the convective boundary. This mixing efficiency is the result of a hydrodynamic convective-reactive phase in which local mixing of the H and  $^{12}\text{C}$  interacts with nuclear burning. This is locally an inherently three-dimensional process that requires calibrated mixing models to be included into one-dimensional simulations. The exact nature of this hot dredge-up mixing will critically determine the subsequent evolution of EMP AGB stars. Similar to the convective boundary simulations presented in the next section, numerical hydrodynamic experiments to study the nature of hot dredge-up mixing in EMP AGB stars are now within reach, and we plan to carry those out in the near future. These simulations will provide valuable insight into the s-process in EMP AGB stars and for the fate of intermediate mass EMP stars during the TP-AGB phase. The hot dredge-up may be related to the observational paucity of NEMP stars.

## H-ingestion flashes (HIF)

From what we have said so far about the s process it is clear that there is presently considerable uncertainty about where and how the heavy slow neutron-capture elements are made in EMP AGB stars. Future stellar evolution calculations have to clarify if the temperature at the bottom of the convective envelope during the third dredge-up is low enough in the lowest mass AGB stars so that the  $^{13}\text{C}$ -pocket for the radiative s-process can form. It also remains to be seen what the role of the convective  $^{22}\text{Ne}$  neutron source is in the low-mass EMP AGB stars, as it is of primary nature. Its effect although marginal in solar-like metallicity AGB stars may be important at these extremely low metallicities, possibly even allowing the primary formation of Fe seeds for heavy-element production [29].

However, there is another important alternative, or additional production site for the s process in EMP AGB stars to be investigated. Several authors have described the H-ingestion flash (HIF) in thermal pulse stars of extremely low metallicity [e.g. 30, 31, 32, 33, 24]. The HIF is related to the hot dredge-up described above. While

in the latter situation protons are mixed from the convectively unstable envelope into the radiative  $^{12}\text{C}$ -rich core, the HIF relates to the situation when protons are entrained from a radiative layer into the He-burning convection zone, either during the He-core flash on the tip of the RGB [e.g. 34, 35], the He-shell flash in thermal pulse AGB or even in some massive star models of zero metallicity during the He-core burning. HIFs occur at extremely low metallicity because of a minimal entropy barrier between the He-burning and hot H-burning layers. The large temperature of the latter is a result of the low abundance of CNO catalytic material for H-burning. HIFs are also known to happen in solar-like metallicity environments. Post-AGB stars that have evolved through the central-star of planetary nebulae phase may experience the HIF as a very-late thermal pulse as young white dwarfs [36, and reference therein]. Observed stellar matches are the born-again stars, as for example Sakurai's object [37]. Other examples include accreting white dwarf that may be SN Ia progenitors [38], the post-RGB late He-flashers [39] or even the X-ray burst phenomenon [40]. However, the HIF may be especially important in the EMP AGB star environment as it provides a neutron rich environment which may be playing the possibly dominant role in the s-process nucleosynthesis in the most metal-poor AGB stars. Iwamoto et al. [41], building on concepts layed out previously by Malaney [42], has tentatively analysed this s-process environment with interesting observable consequences.

### HIFs and hot dredge-up in massive stars

Convective-reactive events very similar to the HIF and hot dredge-up discussed so far for AGB stars are encountered in stellar evolution models of zero or extremely low metallicity massive stars [43]. After the end of He-core burning the convective instability of the extended H-burning shell spreads inward in Lagrangian mass coordinate. Eventually the bottom of this convective zone at which vigorous H-shell burning takes place will be in immediate contact with the radiative layer underneath in which He-burning has produced a small amount of primary  $^{12}\text{C}$ . This amount of  $^{12}\text{C}$  is sufficient to instantaneously enhance the effective rate of H-burning if brought into contact with the burning shell.

In stellar evolution calculations great care has to be taken to numerically resolve the convective boundary. Instantaneous mixing inside the convection zone without any mixing model for the boundary is not resolvable in one-dimensional stellar evolution calculations, and may easily lead to erratic and unphysical model results. Mixing may be minimal at convective boundaries in massive star stellar interiors, and formally it can be made as small

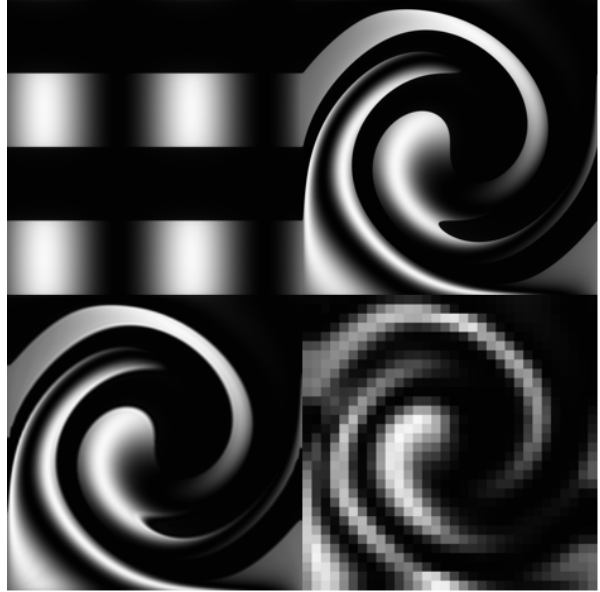


**FIGURE 2.** A 2-D advection test of the PPB scheme. In the upper panels, the initial distribution (left) and final one (right) are shown on a  $1024^2$  grid. At the bottom left and right we show the final distributions on grids of  $128^2$  and  $16^2$ , using the 6 moments updated by the scheme in each grid cell to generate average values in cell quadrants.

as one can numerically afford to resolve. However, if we take the interior convection simulations of C- and O-shell burning of Meakin and Arnett [44] as any guidance, then such mixing at convective boundaries may not at all be minimal. The effect of this convective boundary mixing has already been shown to be significant on the subsequent supernova explosion at solar-like metallicity [45], and it can be expected that similar mixing at all convective boundaries with their respective efficiencies will be even more significant at the low metal content of the first stars.

HIF-like events can also be encountered in massive first stars when the He-core burning convection zone entrains H from the overlying radiative layers (S. Ekström, priv. com.). HIF and hot dredge-up type convective-reactive events can be initiated by rotationally induced mixing [46], and are routinely found in such stellar models. These convective-reactive phases may be especially relevant to nucleosynthesis in extremely metal-poor massive stars, for example for investigating the LEPP (see Introduction) as this mixing determines how much primary  $^{13}\text{C}$  and  $^{14}\text{N}$  is produced as a neutron source for heavy element production.

## Why the need for three-dimensional simulations

One-dimensional stellar evolution models of the HIF in AGB stars, e.g. those by Herwig [24] or Iwamoto et al. [41], are based on two assumptions that are not obviously appropriate for convective-reactive events. These are spherical symmetry and mixing as a diffusion process. Convective mixing is not a diffusion but rather an advection process. The introduction of the diffusion formalism to treat mixing, e.g. in Herwig et al. [47], was motivated by the finding of Freytag et al. [48] that overshoot mixing outside the formally unstable convection zone behaves like diffusion. However, relying on diffusion for the mixing framework in convective-reactive situation inside the unstable region [as for example in 24] is at least questionable. Spherical symmetry can be broken on a global scale, as for example by very fast rotation, and this is why 1D stellar evolution often assumes in such cases a shellular rotation law [49]. One may assume that a HIF is still well described by global spherical symmetry, although even that is not clear. H-deficient high-velocity (200km/s) knots are moving away from the H-deficient planetary nebula central stars Abell 30 and Abell 78 [50] in an otherwise H-normal PN. These two stars are believed to be post-very late thermal pulse stars (see above), i.e. a HIF in a pre-white dwarf. If the knots are ejections that originate HIF hydrodynamics then this could imply that global spherical symmetry is violated in the HIF. On a local scale spherical symmetry is questionable because the assumption that the H-abundance is exactly homogeneous on shells has not been shown to be valid. The answer to this question lies in the competing effect of small scale turbulent mixing that enforces homogeneity and the large-scale convective motions that generate inhomogeneities. He-shell flash simulations of Herwig et al. [26], or the 2D simulation discussed below may indicate that convective downdrafts contain locally more entrained H compared to upwelling material that originates at the He-burning convection zone bottom. This difference leads to a patchiness of the H abundance in any given horizontal plane, resulting in a patchiness of the energy generated from proton captures by  $^{12}\text{C}$ . Fig. 1 demonstrates this effect through inhomogeneities in horizontal planes of a toy model. This needs to be studied quantitatively in properly resolved simulations with the aim to investigate how thick the H-burning layer is, and how the burning products  $^{13}\text{N}$  and  $^{13}\text{C}$  will be distributed in the He-intershell. For the same reasons we need to extend hydrodynamic simulations also to the hot dredge-up episodes, in both intermediate and massive stars.

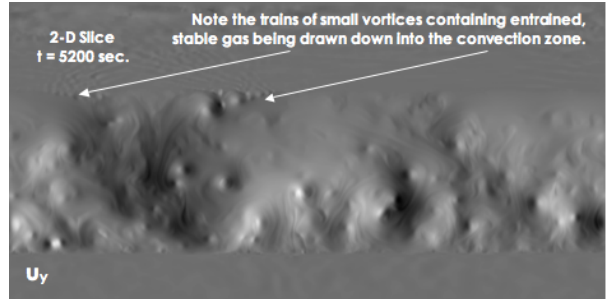


**FIGURE 3.** A 2-D simulation of turbulent convection in the helium shell flash convection zone of a two-solar-mass AGB star. The initial 1-D base state about which this PPM code computes the perturbation resulting from simulated helium shell flash energy input approximates closely the 1-D stratification from the stellar evolution simulation. In this image the vertical component of the velocity is displayed. This  $1024 \times 512$  grid reveals trains of small vortices that form at the top of the convection zone where the gas descends. This is the region and the characteristic flow pattern that we have used to initialize our 3-D PPM simulations reported in the next section.

## STELLAR INTERIOR HYDRODYNAMICS SIMULATIONS

A first step toward comprehensive simulations of the HIF are simulations of the top boundary of the He-shell flash convection zone where the proton-rich material will be entrained. The exact nature of mixing at this boundary determines the rate of H-ingestion as the convective shell makes first contact with the H-rich radiative layer above.

### The numerical technique

*A fully compressible, explicit PPM code for low-Mach number flows*

Our simulations are carried out with an explicit gas dynamics code, multifluid PPM, or PPMF, which accurately tracks sound wave signals even at the low Mach numbers of about up to  $1/30$  that are found in convective gusts. We do this of course, because these are the tools we have at hand. However, a non-directionally-split gas dynamics algorithm must involve roughly 3 times as much work as a directionally split one if it is to achieve the same accuracy. If such a method is made implicit, and only such methods can be made implicit, then an additional cost per time step of at least a factor of 2 results. This means that explicit codes are cost competitive down to at least Mach  $1/6$ , and probably down to Mach  $1/10$  as a practical rule of thumb. Our PPM code has a special implementation in terms of 1-D passes using short vector lengths of 16 exclusively on 128-byte quad-



word operands, which delivers very high levels of performance, exceeding one useful flop per clock tick per processor core with all costs of the code included. It is doubtful that an implicit algorithm, without this 1-D operator decomposition and computational intensiveness, could enjoy this same level of performance. We therefore believe that our computational approach is cost effective, despite the large number of time steps we need in these stellar hydrodynamics problems.

Our version of PPM [cf. 51] modifies the monotonicity constraints in the original PPM so that they are not invoked at all in smooth regions of the flow. This more careful treatment results in considerable improvements in low Mach number flows, which do not contain the shock-generated discontinuities that motivated the constraints in the original scheme. We also note that PPM, unlike methods that use linear interpolation, does not decrease appreciably in accuracy with decreasing Courant number. The reason for this is its elaborate, high-order interpolation of the values at the edges of grid cells, which assume a paramount importance in explicit computations of low Mach number flows. This insensitivity to Courant number is shared by the multifluid tracking algorithm in PPM, PPB, which is described below.

#### *The PPB advection scheme*

The relative concentrations by volume of the two fluids in our problem are tracked by the PPB advection scheme [52], which is a properly constrained, 3-D extension of van Leer's 1-D, unconstrained Scheme VI [53]. The scheme as described by Woodward [52] has been substantially improved, increased in efficiency, and much more carefully constrained over the years since that article, and it has been implemented as a module of the XRAGE production code at Los Alamos in 2004. It has roughly triple the resolving power of PPM advection, due to its use of triple the amount of independent information in each 1-D pass. This extra information comes in the form of low-order moments of the distribution of the fractional volume variable in each cell. In 3-D, 10 such moments are carefully updated by the scheme using 1-D passes, like the host gas dynamics scheme, PPM. These 10 moments serve to define a parabola along any line within the cell for the fractional volume variable (they define a 10-coefficient quadratic form). The updating of the moments is by conservation laws, which results in powerful special properties for the scheme [see 52]. We apply the PPB scheme to fractional volume advection here, and as a result we take very special care to handle the constraints applied to the implied quadratic form in the cell so that sudden transitions of this variable between the special values of 1 and 0 are properly represented. These constraints are far less dramatic than those

involved in PPM's contact discontinuity detection and steepening algorithm, and they deliver the same one-cell effective thickness of a fluid edge without anything like the side effects that contact discontinuity steepening can cause. We have observed these benefits in numerous tests over many years. Here we give only a single representative example.

In Fig. 2 we show the results of 2-D advection in a swirling flow field similar to that encountered in our stellar hydrodynamics problem. The initial distribution has smooth sine wave components in one dimension and relatively sharp, but not discontinuous components in the other. The initial distribution is a product of a sine wave in  $x$  and the 16th root of the absolute value of a sine wave in  $y$ , with the proper sign of the sine wave in  $y$  restored. The variation is then scaled to go from 0 to 1. The sudden jumps in this distribution, shown in the upper left-hand panel of Fig. 2, do not go between the special values of 0 and 1. Their treatment therefore reveals the very small extent to which Gibbs phenomena tend to reduce the faithfulness of this scheme's representation of jumps that do not go between the special values that are so carefully treated. The flow field vanishes at the center and at the edges of the square domain, and thus this advection problem is nonlinear. The results at the initial and at a subsequent time are shown on grids of  $1024 \times 1024$ ,  $128 \times 128$ , and  $16 \times 16$  cells. To generate these displays, we have used the moments of the distribution within the cells that are updated by the PPB scheme (in 2-D we use 6 moments) to generate average values of the distribution in the 4 quadrants of each grid cell. In the displays, each such quadrant is represented by a constant value, so that the individual quadrants and the resolution of the grid can thus be immediately perceived.

## **Numerical Experiments in 2D**

Numerical experiments in 2D motivate the initialization of a 3-D experiment. We first briefly summarize 2-D simulations of the helium shell flash convection zone of a two-solar-mass star about a month before the peak of the helium shell luminosity and before the convection zone has had a chance to expand very much in radius (this is the same 1-D initial state used in the simulations reported in [13]). In Fig. 3 we see a display of the vertical component of velocity in our simulation with the PPM code. Here we use a fine grid of  $1024 \times 512$  uniform grid cells. We also deal with the several orders of magnitude variation with height of the pressure and density by subtracting out from the governing equations the hydrostatic, 1-D base state and computing only the perturbation about it. The bottom of the convection zone, which is easy to make out in Figure 2, is at a radius of 9150

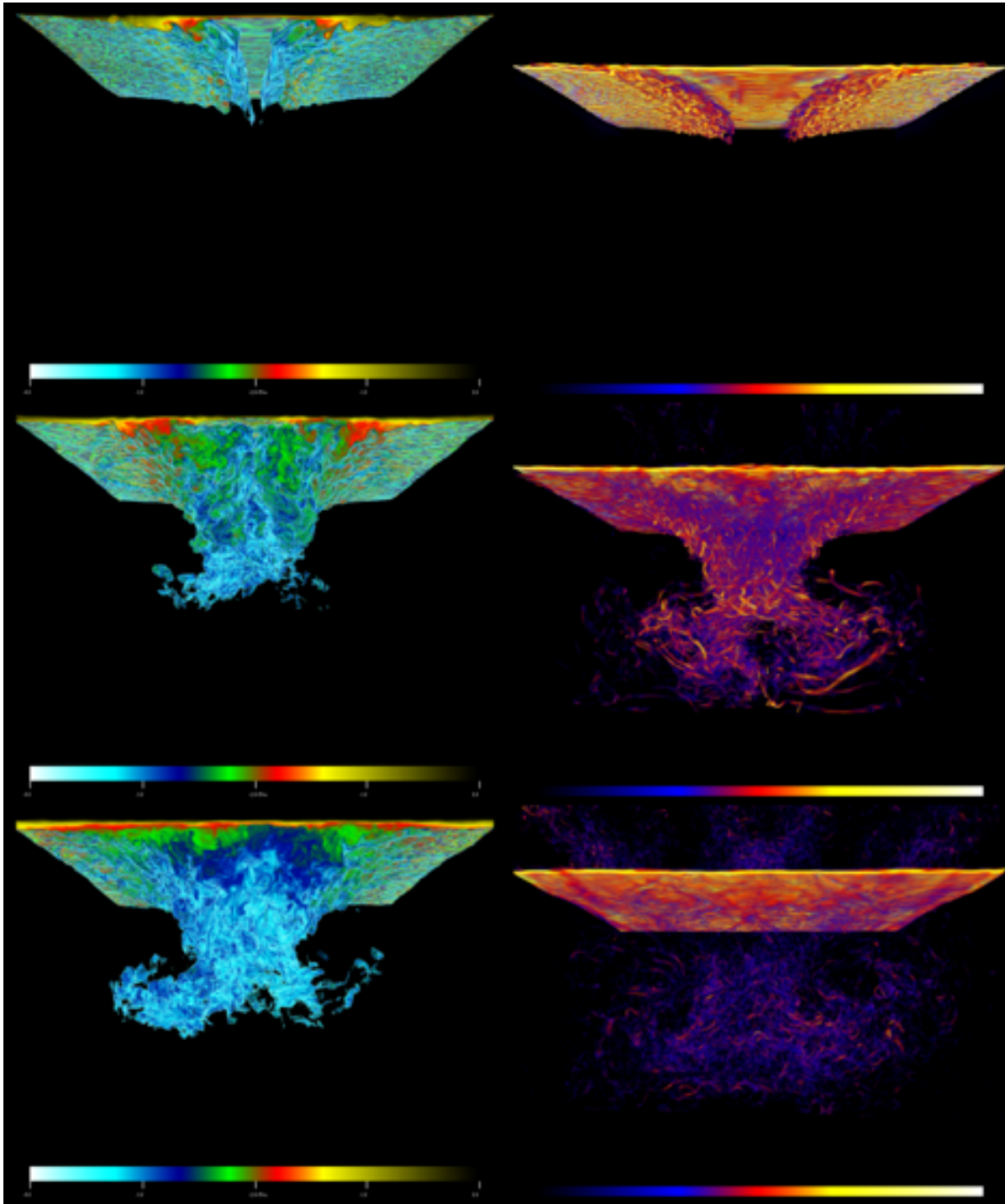


**FIGURE 4.** A 3-D simulation of entrainment of stably stratified hydrogen and helium gas mixture into the 2.26 times denser helium and carbon mixture of the helium shell flash convection zone below it (see discussion in text). The fractional volume images show mixing ratios by volume of 1 part in  $10^4$  as aqua, 1 part in  $10^3$  as blue, 1 part in 100 as red, and 1 part in ten or higher mixing fractions are yellow. Cells containing only pure upper gas are transparent.

km, and the top, also easily discernable, is at 15,200 km radius. At this time, the hydrogen-rich envelope begins at radius 17,500 km. The Mach number of this flow is, at its highest 0.035, which makes this explicit computation relatively expensive, although this calculation was easily performed on a single desktop PC. This 2-D flow shows the tendency for gas from the stably stratified layer above to be entrained at those places where large convection cells flow along the top of the convection zone and begin to descend. Trains of small vortices formed due to shear instabilities are seen descending with the general flow in these regions, potentially carrying a bit of the stably stratified upper gas along inside them. Because the low Mach number of this flow introduces some computational expense in 3D, we chose to include in our 3-D simulation domain only the portion of the convection zone where we expect this entrainment to occur. We use periodic boundary conditions in the two horizontal dimensions, and we, admittedly artificially, introduce reflecting walls at the top and bottom of the domain. We place the top of the convection zone at the middle height in our problem domain, which then extends 100km down into the helium shell flash convection zone below and an equal distance above the top of this convection zone. In the convection zone, we introduce two Mach 1/30, counter-rotating, horizontally oriented large vortices with an initially approximately incompressible flow field and filling the region between the top of the convection zone and the bottom of our grid. We also introduce perturbations near the top of the convection zone in the vertical component of the velocity with sinusoidal variation in modes 1, 3, and 5 in the x-direction along the length of the convective rolls. To stimulate shear instabilities in this dimension, we also introduce a small shear in the x-component of the velocity at the top of the convection zone. We will see below that due to the stable stratification above the top of the convection zone, this shear in x-velocity has little effect in comparison to the behavior induced by the convective rolls. We take the fluid states above and below the top of the convection zone from later in the 1-D stellar evolution, when above this mid-plane in our domain we have mainly hydrogen and helium while below it we have mainly helium and carbon with a density jump of a factor of 2.26 across the midplane (the top of the convection zone). The gas everywhere has a gamma-law equation of state with a gamma of 5/3.

### Results of a 3-D Numerical Experiment

Visualizations of the fractional volume of the upper gas are shown at the left in Fig. 4, and visualizations of the vorticity are shown at the right at the same times, although from a different viewpoint. These simulations

show the capability of this 3-D approach. Preliminary quantitative analysis indicates a partially mixed boundary layer (10 – 15km) in which the abundance of the H-rich mix from the top stable layer drops in horizontal averages from unity to below  $\sim 10^{-4}$  after 20s simulated time, which is about 1/30 of the convective turn-over time scale. Significant inhomogeneities are present in the mix layer with the most enriched downdrafts having maximum H-rich material abundances of  $10^{-2} \dots 10^{-3}$  at depth of 40 to 50km below the boundary. Although these results are based on a set of three simulations with grids of  $256^3$ ,  $512^3$  and  $1024^3$  convergence tests have not been finalized.

These 3-D simulations are meant to study mixing due to the shear at convective boundaries that is induced by horizontal motions driven by convection. The vertical momentum component is zero in this setup. However, a simulation that contains the full convection zone perturbations of the boundary will also include vertical components on larger scales, and in fact these perturbations excite the internal gravity wave spectrum that is observed in the stable layers above and below the convection.

Thus, mixing as found in these simulations applies to what are rather small scales in the full convection simulations. Nevertheless, even with these assumptions we find that notable amounts of material cross the convective boundaries. Here, as a result of our initialization of this problem, we do not observe substantial distortion of the upper boundary of the convection zone by the motions below it. Instead we entrain buoyant gas from the region above this boundary by essentially scraping off bits of it and mixing it into the lower fluid that is moving past. This mixing allows the flow to carry the more buoyant fluid down into the convection zone. When the entrained fluid is hydrogen rich, even if it becomes only a trace constituent of the descending gas it can release significant amounts of energy through nuclear burning.

### ACKNOWLEDGMENTS

The work reported here has been supported at the University of Minnesota by grant DE-FG02-03ER25569 from the MICS program of the DoE Office of Science, by NSF equipment grants CNS-0224424 and CNS-0421423, and by the Minnesota Supercomputing Institute, a part of the University of Minnesota's Digital Technology Center. Funding for this work was also provided through EU Marie Curie grant MIRG-CT-2006-046520. FH is Affiliate of the Theoretical Astrophysics Group in T-Division at LANL, and acknowledges continued collaborative support. We would like to thank Raphael Hirschi for extremely useful discussions. Brian O'Shea and the other organizers of the FSIII meeting have to be thanked for their enormous flexibility to deal with various last-



minute issues we imposed on them.

## REFERENCES

1. A. Frebel, J. L. Johnson, and V. Bromm, *MN* **380**, L40–L44 (2007).
2. T. C. Beers, and N. Christlieb, *ARAA* **43**, 531 (2005).
3. W. Aoki, A. Frebel, N. Christlieb, J. E. Norris, T. C. Beers, T. Minezaki, P. S. Barklem, S. Honda, M. Takada-Hidai, M. Asplund, S. G. Ryan, S. Tsangarides, K. Eriksson, A. Steinhauer, C. P. Deliyannis, K. Nomoto, M. Y. Fujimoto, H. Ando, Y. Yoshii, and T. Kajino, *ApJ* **639**, 897–917 (2006).
4. J. G. Cohen, S. Shectman, I. Thompson, A. McWilliam, N. Christlieb, J. Melendez, F.-J. Zickgraf, S. Ramírez, and A. Swenson, *ApJ Lett.* **633**, L109–L112 (2005).
5. S. Lucatello, T. C. Beers, N. Christlieb, P. S. Barklem, S. Rossi, B. Marsteller, T. Sivarani, and Y. S. Lee, *ApJ Lett.* **652**, L37–L40 (2006).
6. W. Aoki, T. C. Beers, N. Christlieb, J. E. Norris, S. G. Ryan, and S. Tsangarides, *ApJ* **655**, 492–521 (2007).
7. T. C. Beers, T. Sivarani, B. Marsteller, Y. Lee, S. Rossi, and B. Plez, *AJ* **133**, 1193–1203 (2007).
8. S. Lucatello, S. Tsangarides, T. C. Beers, E. Carretta, R. G. Gratton, and S. G. Ryan, *ApJ* **625**, 825–832 (2005).
9. J. A. Johnson, F. Herwig, T. C. Beers, and N. Christlieb, *ApJ* **658**, 1203–1216 (2007).
10. J. J. Cowan, and C. Sneden, *Nature* **440**, 1151–1156 (2006).
11. C. Travaglio, R. Gallino, E. Arnone, J. Cowan, F. Jordan, and C. Sneden, *ApJ* **601**, 864–884 (2004).
12. F. Montes, T. C. Beers, J. Cowan, T. Elliot, K. Farouqi, R. Gallino, M. Heil, K. Kratz, B. Pfeiffer, M. Pignatari, and H. Schatz, 2007, to appear in *ApJ*, arXiv:astro-ph/0602459.
13. C. Chiappini, R. Hirschi, G. Meynet, S. Ekström, A. Maeder, and F. Matteucci, *A&A* **449**, L27–L30 (2006).
14. A. Heger, N. Langer, and S. E. Woosley, *ApJ* **528**, 368–396 (2000).
15. R. Hirschi, G. Meynet, and A. Maeder, *A&A* **443**, 581–591 (2005).
16. F. Herwig, N. Langer, and M. Lugaro, *ApJ* **593**, 1056–1073 (2003).
17. C. Travaglio, R. Gallino, M. Busso, and R. Gratton, *ApJ* **549**, 346–352 (2001).
18. S. W. Campbell, *Structural and Nucleosynthetic Evolution of Metal-poor and Metal-free Low and Intermediate Mass Stars*, Ph.D. thesis, Monash University, Australia (2007).
19. S. W. Campbell, and J. C. Lattanzio, *ArXiv e-prints* **709** (2007), 0709.4567.
20. J. P. Cox, and R. T. Giuli, *Principles of stellar structure*, Gordon and Breach, 1968.
21. D. H. Porter, and P. R. Woodward, *ApJS* **127**, 159–187 (2000).
22. J. A. McSaveney, P. R. Wood, M. Scholz, J. C. Lattanzio, and K. H. Hinkle, *MNRAS* **378**, 1089–1100 (2007).
23. R. Gallino, C. Arlandini, M. Busso, M. Lugaro, C. Travaglio, O. Straniero, A. Chieffi, and M. Limongi, *ApJ* **497**, 388 (1998).
24. F. Herwig, “CNO in Low- and Zero-Metallicity AGB Stars,” in *CNO in the Universe*, ASP Conf. Ser. 2003, astro-ph/0212366.
25. F. Herwig, *ApJ* **605**, 425–435 (2004).
26. F. Herwig, B. Freytag, R. M. Hueckstaedt, and F. X. Timmes, *ApJ* **642**, 1057–1074 (2006).
27. S. Goriely, and L. Siess, *A&A* **421**, L25–L28 (2004).
28. M. Lugaro, F. Herwig, J. C. Lattanzio, R. Gallino, and O. Straniero, *ApJ* **586**, 1305–1319 (2003).
29. L. Husti, R. Gallino, S. Bisterzo, S. Cristallo, and O. Straniero, *Memorie della Societa Astronomica Italiana* **78**, 523–+ (2007).
30. S. Cassisi, V. Castellani, and A. Tornambe, *ApJ* **459**, 298 (1996).
31. M. Y. Fujimoto, Y. Ikeda, and J. Iben, I., *ApJ Lett.* **529**, L25 (2000).
32. A. Chieffi, I. Dominguez, M. Limongi, and O. Straniero, *ApJ* **554**, 1159 (2001).
33. L. Siess, M. Livio, and J. Lattanzio, *ApJ* **570**, 329–343 (2002).
34. D. Hollowell, I. J. Iben, and M. Y. Fujimoto, *ApJ* **351**, 245–257 (1990).
35. H. Schlattl, S. Cassisi, M. Salaris, and A. Weiss, *ApJ* **559**, 1082–1093 (2001).
36. K. Werner, and F. Herwig, *PASP* **118**, 183–204 (2006).
37. P. A. M. van Hoof, M. Hajduk, A. A. Zijlstra, F. Herwig, A. Evans, G. C. van de Steene, S. Kimeswenger, F. Kerber, and S. P. S. Eyres, *A&A* **471**, L9–L12 (2007).
38. S. Cassisi, I. J. Iben, and A. Tornambe, *ApJ* **496**, 376–+ (1998).
39. T. M. Brown, A. V. Sweigart, T. Lanz, W. B. Landsman, and I. Hubeny, *ApJ* **562**, 368–393 (2001).
40. A. L. Piro, and L. Bildsten, *ApJ* **663**, 1252–1268 (2007).
41. N. Iwamoto, T. Kajino, G. J. Mathews, M. Y. Fujimoto, and W. Aoki, *ApJ* **602**, 378–388 (2004).
42. R. A. Malaney, *MNRAS* **223**, 683–707 (1986).
43. M. Limongi, A. Chieffi, and O. Straniero, *MemSAI* **72**, 289–298 (2001).
44. C. A. Meakin, and D. Arnett, *ApJ Lett.* **637**, L53–L56 (2006).
45. P. A. Young, C. Meakin, D. Arnett, and C. L. Fryer, *ApJ Lett.* **629**, L101–L104 (2005).
46. R. Hirschi, *A&A* **461**, 571–583 (2007).
47. F. Herwig, T. Blöcker, D. Schönberner, and M. F. El Eid, *A&A* **324**, L81–L84 (1997).
48. B. Freytag, H.-G. Ludwig, and M. Steffen, *A&A* **313**, 497 (1996).
49. G. Meynet, and A. Maeder, *A&A* **321**, 465–476 (1997).
50. K. J. Borkowski, J. P. Harrington, Z. Tsvetanov, and R. E. S. Clegg, *ApJ Lett.* **415**, L47–L50 (1993).
51. P. R. Woodward, “The PPM Compressible Gas Dynamics Scheme,” in *Implicit Large Eddy Simulation, Computing Turbulent Fluid Dynamics*, edited by L. M. F. Grinstein, and W. Rider, Cambridge University Press, 2006, available at <http://www.lcse.umn.edu/ILES/PPM-for-ILES-turb-apps-2-26-05-cup6a-10.pdf>.
52. P. R. Woodward, “Numerical Methods for Astrophysicists,” in *Astrophysical Radiation Hydrodynamics*, edited by K.-H. Winkler, and M. L. Norman, Reidel, 1986, pp. 245–326, available at [http://www.lcse.umn.edu/projects/34/34\\_PPMlogoPaper.pdf](http://www.lcse.umn.edu/projects/34/34_PPMlogoPaper.pdf).
53. B. van Leer, *Journal of Computational Physics* **23**, 276–299 (1977).